Elsevier Editorial System(tm) for Catena
Manuscript Draft

Manuscript Number:

Title: Short-term geomorphic analysis in a fluvial disturbed environment by fusion of LiDAR, colour bathymetry and dGPS survey

Article Type: Research Paper

Keywords: Fluvial processes; gravel-bed river; colour bathymetry; LiDAR data; floods.

Corresponding Author: Mr. Johnny Moretto,

Corresponding Author's Institution: University of Padova

First Author: Johnny Moretto

Order of Authors: Johnny Moretto; Emanuel Rigon, PhD; Luca Mao, PhD; Fabio Delai; Lorenzo Picco, PhD; Mario A Lenzi, Professor

Abstract: Estimating bed surface elevations underwater results in high uncertainty without the use of bathymetric sensors. In our study, a revised approach has been developed in order to create more accurate and detailed Digital Terrain Models (DTMs) by merging LiDAR data for the dry area, with water depth of wet areas derived from a predictive depth-colour relationship. A regression model was implemented that related water depth and intensity of the three colour bands derived from aerial photos. More than 2400 in-channel depth calibration points were taken through a dGPS survey in a wide range of underwater bed forms. LiDAR and depth points were merged and interpolated into a DTM. The resulting DTMs closely matched the field-surveyed ground surface (average error of ± 19 cm with respect to dGPS sections). The method was applied on three sub-reaches of a north-eastern Italian gravel-bed river (Brenta) before and after two consecutive flood events in 2010, with recurrence intervals of 8 and 10 years, respectively. A severe flood event seems to generate riffle-pool migrations in the case with no- nearby natural or -artificial constriction, while a pool enlargement along the channel when they are beside a constriction.

Dear Editor of Catena Jurnal,

Please find attached a manuscript submission entitled **"**Short-term geomorphic analysis in a fluvial disturbed environment by fusion of LiDAR, colour bathymetry and dGPS survey**".**
The present paper proposes the implementation of a revised methodology for the production of high resolution DTMs of gravel-bed rivers starting from LiDAR surveys which are, generally, associated to aerial images taken during the flight. The work is aimed at evaluating geomorphic changes in the Brenta River as a consequence of flood events occurred in November and December 2010. The specific objectives can be summarized as follows: I) to determine physical and empirical relationships between channel depth and colour intensity and verify which of these variables have more explicative capacity; II) to define factors that increase uncertainty in the final DTMs derived by merging LiDAR data and colour bathymetry data, in order to obtain Hybrid DTMs (HDTMs) at high resolution and low uncertainty; III) to analyze the bed-form changes after severe floods.

The results obtained are a valuable support for planning and management of river morphological recovery.

We hope you could accept our manuscript submission.

Best regards,
Dr Johnny Moretto

Short-term geomorphic analysis in a fluvial disturbed environment by fusion of LiDAR, colour bathymetry and dGPS survey

J. MORETTO[1], E. RIGON[1], L. MAO[2], F. DELAI[1], L. PICCO[1], M. A. LENZI[1]

1 Department of Land, Environment, Agriculture and Forestry, University of Padova, Padova (Italy); University of Padova- AGRIPOLIS-35020 LEGNARO (PD), ITALY

2 Departamento de Ecosystems and Environment; Pontificia Universidad Catolica de Chile; Santiago, Chile

Corresponding author: Johnny Moretto

e-mail: johnny.moretto@studenti.unipd.it;

fax: 0039 (0)498272750;

Address: Campus di Agripolis Viale dell'Università, 16. 35020 - Legnaro Padova (Italy).

Abstract

Estimating bed surface elevations underwater results in high uncertainty without the use of bathymetric sensors. In our study, a revised approach has been developed in order to create more accurate and detailed Digital Terrain Models (DTMs) by merging LiDAR data for the dry area, with water depth of wet areas derived from a predictive depth-colour relationship. A regression model was implemented that related water depth and intensity of the three colour bands derived from aerial photos. More than 2400 in-channel depth calibration points were taken through a dGPS survey in a wide range of underwater bed forms. LiDAR and depth points were merged and interpolated into a DTM. The resulting DTMs closely matched the field-surveyed ground surface (average error of ± 19 cm with respect to dGPS sections). The method was applied on three sub-reaches of a north-eastern Italian gravel-bed river (Brenta) before and after two consecutive flood events in 2010, with recurrence intervals of 8 and 10 years, respectively. A severe flood event seems to generate riffle-pool migrations in the case

with no- nearby natural or -artificial constriction, while a pool enlargement along the channel when they are beside a constriction.

Keywords Fluvial processes; gravel-bed river; colour bathymetry; LiDAR data; floods.

1. INTRODUCTION

The study of river morphology and dynamics is essential for understanding the factors determining sediment erosion, transport and deposition processes. Natural (e.g. climatic and hydrological variations) and anthropic factors (e.g. water captures, grade-control works, gravel mining deforestation) can act at both reach- and basin-scales to change the magnitude or timing of these processes (Buffington, 2012). The geomorphic variations at the reach scale are a direct consequence of sediment erosion and deposition, which are influenced by the size and volume of sediment supply, transport capacity of the flow and local topographic constraints. The quantification of the interaction of these processes is limited by the difficulty of collecting high spatial resolution data in river environments. Traditional approaches based on the application of hydraulic formulas at cross-sections fail when aiming to describe non-uniform natural conditions. Three-dimensional and high-resolution representations of river bed morphology are used in many applications: hydraulic and cellular modelling (e.g. Rumsby *et al.*, 2008); impact evaluation of climate change (e.g. Rumsby and Macklin 1994.); flood hazard management (Macklin and Rumsby, 2007); defining hazardous areas which also involves an assessment of erosion and deposition areas along the river corridor (Stover and Montgomery, 2001; Lane *et al*., 2007). Calculating sediment budgets and estimating sediment transport rates are also fundamental to quantify geomorphological changes due to flood events and changes in flow regime (Ashmore and Church, 1998).

The traditional techniques of terrain survey (e.g. total station devices, dGPS) for evaluating morphological changes in large areas have been demonstrated as being expensive, time-consuming and difficult to apply in areas with limited accessibility. Some innovative methods have shown a good capacity in the production of high-resolution Digital Terrain Models (DTM) of fluvial systems. Recent studies on morphological channel changes have used passive remote sensing techniques such as digital image processing (e.g. Forward Image Model, Legleiter and Roberts, 2009), digital photogrammetry (Dixon *et al*., 1998; Heritage *et al*., 1998; Lane *et al*., 2010), active sensors including Laser Imaging Detection and Ranging (LiDAR) (e.g. Hicks *et al*., 2002; 2006; Kinzel *et al*., 2007; Hicks, 2012) and acoustic methods (e.g. Muste *et al*., 2012; Rennie, 2012).

The main difficult related to the production of precise DTMs with non-bathymetric sensors is due to the absorption of natural (solar) or artificial (LiDAR) electromagnetic radiation in the wet channel. The capacity of the electromagnetic signal to pass through water, reflect from the bed and reach a sensor depends on the water surface texture (pleating, reflexes, etc.), the water column (depth and turbidity) and some bed (substrate type and algae presence) characteristics (Marcus, 2012; Marcus and Fonstad, 2008).

Only a few tools have proved able to provide an accurate and high-resolution measure of the submerged bed surface, and survey precision decreases with the increase in water depth. Bathymetric LiDAR sensors have recently been developed and should enable the survey of underwater bed surfaces. Nevertheless, they feature high costs, relatively low resolutions, and data quality comparable to photogrammetric techniques (Hilldale and Raff, 2008). Progress in the LiDAR acquisition of topographic information from submerged areas has been made with a new technology: Experimental Advanced Airborne Research LiDAR system (EAARL) that records the full waveform of the returning laser pulse. This system is affected by environmental conditions (e.g. turbulence in the pool, bubbles in the water column, turbidity, and low-bottom albedo) and post-processing algorithms even if the accuracy appears

comparable to that of airborne terrestrial near-infrared LiDARs (Kinzel *et al*., 2013; McKean *et al*., 2009).

The survey of wet areas can thus be approached using two photogrammetric techniques (manual or automatic) which are able to produce a cloud of elevation points (Rinner, 1969; Fryer, 1983), or with a technique based on the calibration of a depth-reflectance relationship of images, which can be in greyscale (e.g. Winterbottom and Gilvear, 1997), coloured (e.g. Carbonneau *et al*., 2006, Moretto et al, 2013a) or multispectral (Marcus *et al*., 2003; Legleiter, 2011). Both solutions need a field survey, contemporary to the flight, to provide calibration depth points.

The depth-reflectance relationship can be defined using an empirical relationship, using one or more bands (e.g. Legleiter *et al*., 2009), or according to the Beer-Lambert law. In the latter case the amount of light absorbed by a transparent material is proportional to the distance of the light travelling through that material (Carbonneau *et al*., 2006):

$$I_{out} = I_{in}\, e^{-cx} \tag{1}$$

Where l_{in} is the incoming intensity, l_{out} the outgoing intensity, c is the rate of light absorption, and x the distance.

Once reliable digital elevation models (DEMs) have been obtained, it is possible to detect and interpret, in a quantitative way, geomorphic changes in river systems (e.g. Lane *et al.*, 1994). An important component to be evaluated on DEMs is the uncertainty, which can be influenced by many factors. The most decisive error sources include survey point quality, sampling strategy, surface topographic complexity and interpolation methods (Panissod *et al*., 2009; Milan *et al.*, 2011). Total uncertainty is usually derived from the classical statistical theory of errors (Taylor, 1997) where an estimation of DEM accuracy based on survey data is used as a surrogate for DEM quality (Milan *et al.*, 2007).

This paper proposes the implementation of a revised approach for the production of high resolution DTMs of gravel-bed rivers starting from LiDAR surveys and aerial images

acquired during the flight. The aim is to evaluate morphological change patterns in the Brenta River as a consequence of flood events that occurred in November and December 2010. The Brenta river basin, like the majority of Italian rivers (Comiti *et al*., 2011; Surian, 2012), has undergone intense and multiple human impacts starting from phases of deforestation and reforestation, followed by interventions for hydroelectric power generation and irrigation purposes, which have altered both the catchment and the river channel.

The specific objectives can be summarized as follows: I) to determine physical and empirical relationships between channel depth and colour intensity and verify which of these variables have more explicative capacity; II) to define factors that increase uncertainty in the final DTMs derived by merging LiDAR data and colour bathymetry data, in order to obtain Hybrid DTMs (HDTMs) at high resolution and low uncertainty; III) to analyze the bed-form changes after severe floods.

2. STUDY AREA

The Brenta River is located in the South-Eastern Italian Alps, having a drainage basin of approximately 1567 km^2 and a length of 174 km. Average annual precipitation, mainly concentrated in spring and autumn seasons, is about 1100 mm. The geology of the area is rather complex and includes limestone, dolomite, gneiss, phyllite, granite and volcanic rocks.

The study reach is 19.2 km in length and lies between Bassano Del Grappa and Piazzola sul Brenta (Figure 1). The dominant morphologies are wandering and braided, the active channel width varies between 300 m and 800 m, and average slope is about 0.0036 m/m. Within this study reach, three sub-reaches 1.5 km long and 5 km apart were selected as representative of the upper- middle- and down-stream part of the study area and named according to the nearby villages: Nove, Friola and Fontaniva (Figure 1). The upstream sub-reach (Nove) has a single

132 straightened channel morphology with an average width of around 300 m. By contrast, Friola
133 shows a more complex morphological pattern, with the braided channel accounting for high
134 levels of vegetation density and an average width of 500 m. In the downstream sub-reach,
135 Fontaniva, the braided trend is more marked, with the formation of many fluvial islands and
136 the 800 m wide channel divides into several branches.
137 The Brenta river basin has suffered centuries of disturbances, mostly due to deforestation and
138 reforestation. The water course was regulated for hydroelectric power generation and
139 irrigation purposes and dams were built in many parts of the drainage basin, intercepting
140 sediments from more than 40% of the drainage area. Moreover, between 1953 and 1985,
141 gravel was intensively quarried in the main channel and, starting in the 1930s, effective
142 erosion and torrent control works were executed in the upper basin (Bathurst *et al*., 2003;
143 Lenzi *et al*., 2003; Lenzi, 2006; Rigon *et al*., 2008; Conesa-Garcia and Lenzi, 2010; Surian et
144 al., 2009). Human interventions, especially during the second half of the 20th century, have
145 considerably altered the sediment budget of Alpine rivers (Mao and Lenzi, 2007; Mao *et al*.,
146 2009; Comiti, 2011; Comiti *et al*., 2011; Picco *et al*., 2013). As a result of these impacts, the
147 average riverbed width of the Brenta has narrowed from 442 m at the beginning of the 1800s,
148 to 196 m in 2010, and channel incision has ranged from 2 to 8 m, especially due to the effects
149 of gravel quarrying that only ended during the 1990s (Surian and Cisotto, 2007; Moretto *et*
150 *al.*, 2012a, 2012b, 2013b; Kaless *et al*., 2013). In recent times, a new adjustment phase seems
151 to be taking place (channel widened to 215 m in 2011) as evidenced by the expanding trend of
152 the active channel with a contemporary increase in vegetated islands over the last twenty
153 years (Moretto *et al.*, 2012a, 2012b, 2013b). Nevertheless, the river presents several localized
154 variations along its course, which are linked to the different erosion-sedimentation processes
155 underway. The recent evolutionary dynamics differ from those in the past and, since the
156 abandonment of gravel mining activities on the river bed (1990s), there has been a partial
157 morphological recovery, especially in the downstream sub-reach, Fontaniva. However, this

158 trend is still unstable and not distributed along the whole study reach. In the upstream area,
159 there are still incision processes and a widening of the active channel as a result of bank
160 erosion (Moretto *et al*., 2012a, 2012b, 2013b).

161 Two flood events occurred between the LiDAR flights (Figure 2). The November 2010
162 flood reached a maximum average daily discharge of 720 m^3/s, with a slower drop in the
163 water level compared to the second flood event in December 2010, which had the highest
164 discharge of the last 10 years (maximum average daily discharge of 759 m^3/s). The first flood,
165 caused by prolonged and heavy rainfall between the 31st of October and 2nd of November
166 2010, which totalled 300 mm with local maximums over 500 mm (Figure 3), with a
167 recurrence interval (RI) of about 8 years. The Brenta river registered very high hydrometric
168 levels - among the highest ever recorded, and numerous instability events occurred at the
169 basin scale, such as landslides, bank erosion processes and flooding outside the banks. The
170 second flood, originated by intensive precipitations between the 21st and 26th of December
171 that fell mostly in the pre-alpine and piedmont areas, had an RI of about 10 years. Rainfall
172 exceeded 150 mm with local maximums of 300-400 mm and the river registered (at Barzizza
173 station) higher hydrometric levels than the first flood event, probably due to the greater soil
174 saturation at basin scale and, more particularly, the fact that a major reservoir (Corlo) had
175 already been filled by the previous flooding.

176 The return interval of these floods was estimated from the maximum annual values of the
177 mean daily water discharge over 79 hydrological years. The functions of hydrological
178 probability distribution that were tested are: Log Normal, Log Pearson Type III, Frechet, and
179 Gumbel. The Gumbel distribution (OLS) demonstrated the best performance of the
180 Kolmogoroff test. Taking into account the Gumbel distribution and 90% confidence limits, it
181 was possible to establish the flood values associated with the probability of occurrence (Lenzi
182 *et al*., 2010; Kaless *et al*., 2011; Kaless *et al*., 2013).

183

3. MATERIAL AND METHODS

To create an accurate digital terrain model, a regression model was calibrated between the water depth and the Red, Green and Blue (RGB) bands values deriving from aerial images acquired during the LiDAR survey. The water depth was estimated indirectly as the difference between the water surface (estimated from interpolation of selected LiDAR points; see details in section 3.2) and bed elevation (measured with dGPS in the field). Hybrid digital terrain models (HDTM) were then created, derived from the interpolation of LiDAR (section 3.4) points for dry areas and colour bathymetry derived points for wet areas. A total of three HDTMs were developed for each considered year referring to the three sub-reaches (Nove, Friola and Fontaniva).

This process (Figure 4) was divided into five principal steps: (A) LiDAR data and field survey, (B) dataset preparation, (C) bathymetric model determination, (D) HDTMs creation and (E) HDTMs validation. At the end, three DEMs of difference (DoDs - one for each sub-reach) were produced for each year, and the volumetric surface change and relative uncertainty calculated. The details of this process are explained in the sub-sections below.

The novel contribution of this approach mainly regards four aspects:

I) The field of application involves complex depth and colour characteristics (due to high periphyton loads on the channel bottom);

II) A revised methodology to estimate the water depths to associate with the colour bands (depths of calibrations), thanks to the difference between the elevation of the water surface (derived from selected LiDAR points) and that of the channel bottom (derived from a dGPS survey performed contemporarily with the LiDAR survey). In this way the application of the approach is also possible without direct water depth measures;

III) The search for the best depth-colour model, testing existing physical models (based on

Beer Lambert law formula) and empirical models through different statistical regression methods;

IV) The application of filters, based on colour variability analysis, to reduce the errors of the bathymetric models (presence of pheriphyton, light reflections, exposed sediment, shadows, suspended load and water turbulence).

3.1. LiDAR data and field survey

Two LiDAR surveys were conducted on the 23rd of August 2010 by Blom GCR Spa with an OPTECH ALTM Gemini sensor and on the 24th of April 2011 by OGS Company with a RIEGL LMS-Q560 sensor (flying height ~ 850 m). For each LiDAR survey a point density able to generate digital terrain models with 0.5 m of resolution (at least 2 ground points per square metre) was commissioned. The average vertical error of LiDAR was evaluated through dGPS points on the final elevation model. LiDAR data were taken along with a series of RGB aerial photos with 0.15 m pixel resolution. The survey were conducted with perfect weather conditions and low hydraulic channel levels. An in-channel dGPS survey was performed, taking different depth levels in a wide range of morphological units. A total of 882 points were surveyed in 2010 and 1526 points in 2011. Finally, two cross-sections for each sub-reach were surveyed through dGPS (dGPS average vertical error ± 0.025 m). It is important to note that the dGPS survey was performed contemporarily with the LiDAR data to avoid the introduction of additional stochastic components.

3.2. Dataset preparation

The raw LiDAR points cloud was analysed and the ground surface was identified through an automatic filtering algorithm (TerraScan, Microstation Application®) and, in critical areas (such as near bridges), using manual checks. The aerial photos were georeferenced and corrected by applying a brightness analysis using the appropriate tool within the semi-

236 automatic framework TerraPhoto (Microstation application®). The corrected photos were
237 joined (ESRI® ArcGIS 10) and the pixel size was resampled from 0.15 m to 0.5 m to
238 minimize the georeferencing error and reduce the possible strong colour variation due to light
239 reflection, exposed sediment, periphyton, shadows and suspended load. This is a crucial point
240 because poor photo georeferencing can significantly increase the error due to a wrong
241 association between water depth and colour intensity. The choice of improving the pixel size
242 to exactly 0.5 is also in relation to the resolution of the final elevation model (value derived
243 from point density analysis).
244 Wet areas were digitalized through a manual photo-interpretation process. Along the edges of
245 "wet area" shape polygons, LiDAR points able to represent the water surface elevation (*Zwl*)
246 were selected and used to create a water surface elevation raster (Kriging interpolation).
247 Corresponding colour band intensities and *Zwl* were added to the points acquired in the wet
248 areas (dGPS wet-area survey) obtaining a shape file of points containing five fields (in
249 addition to the spatial coordinates x and y): intensity of the three colour bands, Red (*R*), Green
250 (*G*), Blue (*B*), elevation of the channel bed (*Zwet*) and *Zwl*. Finally, channel depth was
251 calculated as $Dph = Zwl - Zwet$. A similar method was employed by Legleiter (2013) using
252 the difference between the mean water surface elevation and the bed elevation, both derived
253 from GPS survey.
254
255 **3.3. Determination of the best bathymetric model**
256 Starting from the obtained dataset, the water depth (estimated indirectly) was considered as
257 the dependent variable, with the three intensity colour bands (R, G and B) as independent
258 variables. 80% of the dataset was used for calibrating the depth-colour model and the
259 remaining 20% to verify the efficiency and choose the best model. Physical models based on
260 the Beer Lambert law (Eq. 1) were tested first.

A ratio-based method was employed to detect changes in depth and filter out the effect of changes in bottom albedo (e.g., Dierssen *et al*., 2003). Legleiter *et al*. (2004) and Marcus and Fonstad (2008) demonstrated that the log-transformation of the red-over-green band ratio correlates linearly with water depth across a wide range of substrate types:

$$DPH = \alpha + \beta_0 ln\,(R/G) \quad (2)$$

where DPH is the water depth, α and β_x are the calibration coefficient, and R and G are the intensities of the red and green bands.

An empirical linear model evaluating all the colour bands, the possible interactions and the square and cubic terms were then tested:

$$DPH = \alpha + \beta_0 R + \beta_1 G + \beta_2 B + \beta_3 RB + \beta_4 RG + \beta_5 GB + \beta_6 RGB + \beta_7 R^2 + \beta_8 G^2 + \beta_9 B^2 + \beta_{10} R^3 + \beta_{11} G^3 + \beta_{12} B^3 \quad (3)$$

Where α and β_x are the calibration coefficients in the depth colour regression. In this model the significance of each component was tested and deleted when the statistical test adopted (explained below) resulted as negative.

The statistical regressions were performed in R® environment using two methods: the traditional regression method based on statistical significance testing of each variable (p-value < 0.05), and the AICc index (Burnham and Anderson, 2002). The second approach estimates all the significant models, forming a ranking founded on the AICc value (the lower value represents the best model), starting from the most complex plausible model. The AICc method automatically deletes the non-significant variables while the deleting process in the first method is manual. The model featuring the lower error was used to build the "raw channel depth raster" (RDPH).

3.4. Hybrid DTM creation and validation

The best bathymetric model was applied to the georeferenced images (raster calculator) to determine the "raw channel depth raster" (RDPH). The RDPH was then transformed into

points (2 points/m^2) and filtered in order to delete wrong or suspicious points, mainly due to sunlight reflection, turbulence, and elements (wood or sediment) above the water surface.

The proposed methodology used for filtering possible wrong points is characterized by an analysis of slope changes in neighbouring pixels. When there are very strong slope changes between neighbouring pixels, a potential error of depth estimation exists. We could analyse these variations through a semi-automatic method that forecasts the creation of a "curvature raster" (ESRI® ArcGIS 10), obtaining a value of curvature (slope derivative) for each pixel. The "range" of curvature to consider a difference of depth between two pixels "real" (with our pixel resolution of 0.5 m) was identified as $-600 < x < 700$. The pixel, with curvature values outside this range were removed, as in this case the "gap" between two pixels is greater than 0.6 m. In addition, the upper and lower implausible limits (outliers; < 5% of total points distribution) were deleted.

On the corrected points (*DPH* model), the corresponding *Zwl* was subtracted to obtain, for each point, the estimated river bed elevation (*Zwet = Zwl -DPH;*). Hybrid DTMs (HDTM) were built up with a natural neighbour interpolator, integrating Zdry points (by LiDAR) in the dry areas and Zwet points (by colour bathymetry) in the wet areas.

Finally, the HDTM models were validated by using dGPS cross-section surveys. The error of each "control point" was derived considering the difference between the elevation of the HDTM and corresponding elevation of the dGPS control point.

The accuracy of the HDTMs was estimated separately for wet and dry areas, also taking into account the dGPS error (available from the instrument for each point).

3.5. Analysis of morphological changes

Thanks to the HDTMs obtained with a precise definition in both dry and wet areas, we were able to explore the effects of severe floods. HDTMs comparison, analysing the dynamics of the bed forms (riffle - pool) as a consequence of flood events and natural and artificial

313 "constrictions", was performed in order to integrate the erosion-deposition patterns analysis
314 described in Moretto *et al*. 2012a for the same study area.
315 Canopy surface models (CSM), derived from the difference between digital surface models
316 (DSM) and DTMs, were produced to identify the natural (fluvial islands) and artificial
317 (embankments and bridges) vertical construction in the analysed sub-reaches. In addition to
318 the bathymetric rasters, three water depth classes (0 – 0.5m; 0.5 – 1m and > 1 m) were
319 applied to identify the different bed forms.

320

321 **4. RESULTS**

322 **4.1. Colour bathymetry models**

323 To understand the variability and average depth of the channel, before calibrating the model
324 regression, the average, standard deviation and maximum depth of 2010 and 2011 wet
325 channels were estimated. 2010 was characterized by an average depth of 0.53 m, a standard
326 deviation of 0.34 m and maximum known depth of 1.62 m. 2011 had a greater average depth
327 than 2010 and equal to 0.63 m, a standard deviation of 0.28 m and maximum known depth of
328 1.63 m.
329 The search for the best depth-colour model started by testing a physical model, based on the
330 Beer Lambert law (Eq. 2) for each year (2010 and 2011) and with the two statistical
331 regression methods (traditional regression and AICc index; Section 3.3).
332 The application of the traditional regression method and the AICc index produced the same
333 depth colour model for 2010:

334 $$DPH = - 0.119 + 2.725 \ln (R/G) \quad (5)$$

335 Where *DPH* is the water depth and *ln(R/G)* are the colour bands arranged according to the
336 Beer Lambert law.

337 This model has a statistically significant p-value << 0.05, r^2 of 0.34 and an average error
338 derived from the test points of ± 0.27 m.
339 A similar result was obtained with the 2011 model; also in this case the two statistical
340 regression methods have produced the same result:

341 $$DPH = - 0.73 + 2.043 \ln (R/G) \quad (6)$$

342 This model has a statistically significant p-value << 0.05, r^2 of 0.25 and an average error
343 derived from the test points of ± 0.20 m.
344 The *depth-colour (RGB)* statistical regressions performed in the empirical model with the two
345 different approaches allowed two bathymetric models to be obtained for each year (2010 and
346 2011). The average errors, detected in the two models by comparing the test points of 2010,
347 are equal to ± 0.26 m and highlighted negligible differences accounting for the same
348 magnitude of the estimation errors (0.003 m of difference of average error). Therefore, the
349 model resulting from the traditional method (reported below; with verified p-value) was
350 preferred because of its simpler structure with fewer factors if compared to the AICc model:

351 $$DPH = 5.31 + 0.07513\,R - 0.1869\,G - 0.01475\,B - 0.0004582\,RB$$

352 $$+ 0.001056\,G^2 + 0.0003352\,B^2 - 0.000002142\,G^3 \quad (7)$$

353 Where *DPH* is the estimated water depth and R, G and B are the red, green and blue bands,
354 respectively. The model presents an r^2 of 0.46, 12 percentage points more than the 2010
355 physical model.
356 In 2011, on the other hand, the two different methodologies (traditional and AICc index) of
357 statistical regression generated the same model:
358

359 $$DPH = -0.607 + 0.03508\,R - 0.06376\,G - 0.1377\,B + 0.002257\,RG - 0.001096\,RB + 0.002303\,GB$$

360 $$- 0.0007273\,R^2 - 0.002956\,G^2 + 0.0009993\,B^2 + 0.000002837\,G^3 - 0.00000685\,B^3 \quad (8)$$

In this case, r^2 is equal to 38%, whereas the estimated depth average error, resulting from the test points, accounts for ± 0.19 m. Both physical and empirical models proved to be statistically significant (p-value << 0.05), but the empirical models seem to have more predictive capacity than the physical model. In addition, all three colour bands significantly contribute to depth estimation, so the presence of interactions between the colour bands (as reported in Figure 5) should be taken into consideration.

We therefore decided to use the empirical models because, despite the similar average errors on the test points, they feature a more predictive capacity than the physical one and also take into consideration the interactions (correlations) between the colour bands.

Figure 6 shows one of the outputs deriving from the model application (Eq. 8) on the Friola sub-reach. It appears that depth variations are generally respected, and variations in the colour tone, due for example to the presence of periphyton in these areas joined to slower water flow, do not seem to strongly influence the estimation of water depth. In this sub-reach, the maximum estimated depth from the models is up to 2 m.

It is important to note that the model error reported above was evaluated comparing the test points, on the 20% of the dataset not used for the statistical regressions. This is therefore not the final error; indeed the next section discusses the effects of the filters (as described in section 3.4) to delete the majority of these errors.

4.2. HDTM production and validation

After filtering raw depth points deemed wrong due to the model application on the altered pixel colour value (caused by river bed colour, water turbulence, light reflections, shadows, suspended load, exposed sediment), dry areas were integrated using the LiDAR flight. The LiDAR points cloud (excluding wet areas) featured an average density of 2.07 points/m^2 for 2010 and 2.64 points/m^2 for 2011; the final HDTMs were generated using a 0.5 x 0.5 m cell size. The final HDTMs, three for 2010 and three for 2011 (Nove, Friola and Fontaniva sub-

387 reaches) are reported in Figure 7. It is worth noting the accuracy in the bed-forms definition
388 (riffles and pools) within the wet channels estimated through the bathymetric process.
389 The data validation (Table 1) was performed separately for both wet and dry areas, obtaining
390 average uncertainty values (by field survey comparison) for each HDTM that include dGPS,
391 LiDAR and DPH estimated errors. The average uncertainty associated to wet areas accounts
392 for from a minimum of ± 0.19 m (Friola 2011) to a maximum of ± 0.26 m (Nove - Fontaniva
393 2010 and 2011), whereas in the dry areas the average uncertainty ranges from a minimum of ±
394 0.14 m (Nove 2010) to a maximum of ± 0.26 m (Fontaniva 2010). The chosen colour
395 bathymetric models (empirical depth-RGB) generated similar error levels for both 2010 and
396 2011. Moreover, the average weighted uncertainty was calculated in the final HDTMs, and
397 ranges from ± 0.16 m (Nove 2010 – 2011 and Friola 2011) to ± 0.26 m (Fontaniva 2010).
398 The last phase of the HDTM production process consists of model validation with dGPS
399 cross-sections. Figure 8 shows an example of comparison of three cross-sections for 2011,
400 obtained with three different types of data (dGPS survey, LiDAR, and HDTM). The section
401 reference is the dGPS, in which the measured points have an average error of about 0.025 m.
402 The main topographical variations result as being faithfully reproduced, except for the
403 thalweg, which was difficult to detect with a dGPS survey. Comparing the dGPS and LiDAR
404 profiles, the inability of the LiDAR signal to penetrate wet areas more than 20 cm was
405 confirmed (with consequent underestimation of the calculated volumes). Instead, comparing
406 dGPS and HDTM profiles, it appears that, overall, the ground points are fairly well replicated**.**
407

408 **4.3. Morphological change detection**

409 From Figure 7 reporting the HDTMs comparison, an interesting change after the floods can
410 be noted: where the main channel had less lateral constriction, it seems to have an increased
411 sinuosity. Indeed, Nove sub-reach is the most constrained laterally due to artificial left
412 enbarkments and also presents the highest incision degree. It therefore has less increase of

sinuosity than Friola and Fontaniva sub-reaches. Comparing these two reaches, Friola presents less change in sinuosity than Fontaniva, probably due to the position next to the artificial banks (on the left side) of the main 2010 channel.

Figure 9 shows the CSMs with pool locations (e.g. P1, P2) on the wet areas of Nove, Friola and Fontaniva sub-reaches in 2010 and 2011. Pools are identified as dark areas, i.e. the zones with the higher water depth with respect to the riffles. It is noteworthy that after the floods, the old pools are longer on average. This phenomenon is particularly evident in Friola sub-reach (pool P3 and P4 2011) and Fontaniva (pool P4 2011). Observing the models, the new pools and the old one still presents do not seem to have formed and evolved in casual positions. The embankments and fluvial islands appear to have played an important role in the bed-form dynamics during the floods. Indeed, the pools in each 2011 sub-reach are located mainly at the side of the wet area with a more compact lateral surface with embankments and/or vegetated bars. On the other hand, riffles are mainly located where no significant "constrictions" were present on either side of the wet areas. The dislocation of the 2010 bed forms does not seem to follow the same principles.

DISCUSSION

5.1. Analysis of the proposed method for geomorphic change detection

The proposed method is a revised procedure for the production of high resolution DTMs on gravel-bed rivers, integrating LiDAR points with filtered bathymetric points estimated through a regression model implemented on wet areas with high heterogeneity.

The bathymetric points can be derived from a physical and empirical relationship between water depth and RGB bands of aerial images taken concurrently with LiDAR data.

438 The model calibration requires a dGPS survey of the water level, without needing direct water
439 depth measurements. It is crucial to acquire dGPS points nearly contemporary to LiDAR and
440 aerial images, as already pointed out by Legleiter (2011). In fact, the calibration of the model
441 does not need direct field surveys of water depth because this is indirectly estimated. Depth
442 estimation entailed the subtraction of the water level raster (water surface) from the
443 corresponding dGPS elevation points (bottom surface) of the channel bed (Zwet). This
444 method is an effective approach for the indirect estimation of water depth and a similar
445 technique was used by Carbonneau *et al.,* (2006). Checking the results obtained from direct
446 measurements of water depth, using gauge rods in correspondence to dGPS points, we noticed
447 that the values obtained from the same points by indirect estimation account for an average
448 error of 0.15 m. This error may also be due to the speed of the water flux during the direct
449 sampling, that created some turbulence around the graduated bar.
450 Indirectly estimated depths (see section 3.2), together with the corresponding RGB values,
451 made up the dataset for the statistical calibration of the regression models. The statistical
452 analysis showed that all three bands (R, G, B) and also some of the other constituent factors
453 (interactions among bands and square and cubic terms) are significant (p-value < 0.05) to
454 predict the water depth. This statistical significance was also confirmed by two different
455 statistical regression methods (verification of p-value and AICc index). The "ad hoc"
456 calibration for each study year was necessary because of the different water stage during the
457 LiDAR survey.
458 This study has demonstrated that in a very heterogeneous wet area, with different depths and
459 different colours on the channel bottom (due to the presence of periphyton), the tested
460 physical models have a lower degree of significance than the empirical models. The empirical
461 models use all the colour bands, and also take into consideration their interactions (non-
462 independence from the explicative variables), the presence of which is demonstrated in Figure
463 5. All the estimated models (physical and empirical) have an r^2 lower than other similar

studies (e.g. Carbonneau *et al.*, 2006; Legleiter *et al.*, 2011), but this is due to the very strong colour and depth variability. Despite a lower r^2, the final validations of the elevation models (shown in Figure 8 and Table 1) have demonstrated a bathymetric uncertainty comparable with the LiDAR data.

Table 2 shows that in our case the optimal application range of the estimated bathymetric models is between 0.2 m and 1.0 m for 2010 and 2011, respectivelly. The error of estimated water depth increases, in the first 20 cm from the water surface, due to strong colour variations at the bottom (periphyton, exposed pebbles, woody debris, etc.). This error was eliminated by substituting those areas with LiDAR points, capable of penetrating this first water layer. The capacity of the LiDAR signal to produce a reliable estimate in the first 20 cm of the water column was confirmed by dGPS and LiDAR cross-section comparison (Figure 8).

Nevertheless, the possible sources of error in the proposed colour bathymetry can generate elevation models of wet areas with an error on our data of less than ± 0.22 m for 95% of the 2010 wet area and less than ± 0.26 m for 99%. For 2011 we obtained an error of less than ± 0.24 m for 80% of the wet area and less than ± 0.32 m for 89%. Hydraulic conditions differed between 2010 and 2011 (see section 4.1), and the number of calibration points can play a significant role especially in a very variable fluvial environment.

To confirm the importance of using a bathymetric method if the aim is to evaluate erosion – deposition patterns by applying numerical models or developing sediment budgets, table 1 reports the loss of volume without applying colour bathymetry. These volumes were derived by subtraction between HDTMs and DTMs (derived entirely from LiDAR). The minimum loss (possible erosion and/or deposition) of 529,813 m^3 is registered at Nove and the maximum of 4,743,783 m^3 in Fontaniva. Therefore the loss of potential erosion and deposition without applying a bathymetric method cannot be excluded to avoid obtaining results far from the reality.

A comparison of the 2011 raw HDTM and the HDTM derived from the profiles of Friola wet areas is shown in Figure 10. Four types of errors were identified on raw HDTM: light reflection, water turbulence, periphyton and exposed sediment (sources of errors highlighted also by Legleiter *et al.*, 2009). The light reflections and water turbulence (white pixels) produce strongly negative depth estimates and substantially different (about 1 - 2 m) from adjacent pixels not affected by these problems. The exposed or nearly exposed periphyton (green and brown pixels) and exposed sediment (grey pixels) produce an underestimation or overestimation of water depth (about ± 0.40 - 0.60 cm of difference with respect to the adjacent pixels). The correction method, which involves the use of a filter based on the curvature and removal of outliers (points with errors exceeding 95% confidence interval), has provided excellent results as evidenced by Figure 10. The proposed filtering approach of erroneous points due to the causes listed above is the new element of the proposed colour bathymetric methodology.

Shadows represent a disturbance factor difficult to correct and remove because they tend to cause an overestimation of the channel depth. However, their presence was minimal in the study sites, thanks to the image acquisition being done at midday. A further limitation is a water depth greater than 1.0 - 1.10 m, where the model tends to produce underestimations. This is partially due to the low availability of calibration points (for safety reasons) in the deepest areas of the water channel. Legleiter (2013) explained that depth estimates through aerial images become less reliable in deeper water due to the increase in saturation of the radiance signal.

In the HDTM profile there are some small areas lower than the dGPS profiles (Figure 8). This may be due, in part, to the presence of large boulders in the water channel that have altered the comparison between precise dGPS measurements and those derived from a mediated profile by HDTM cells of 0.5 x 0.5 m. These deviations are localized and on average included in the total average error detected in this reach (± 0.16 m). Consequently, the HDTMs

produced can be considered a satisfactory topographical representation (considering the resolution of the final elevation models) for a homogeneous study of morphological variations.

5.2. Geomorphic changes after November and December 2010 floods

The morphological evolution of the Brenta River over the last 30 years has been strongly influenced by human impacts and flood events (Moretto *et al*., 2013b). Lateral annual adjustment is directly correlated with the mean annual peak discharge (Moretto *et al*., 2012a, 2013b), thus a higher magnitude of flooding corresponds to greater active channel widening. Substantial increases in channel width and reductions of riparian vegetation occur with flood events with an RI of more than 5 years, as already highlighted by other works concerning similar fluvial environments (e.g. Bertoldi *et al*., 2009; Comiti *et al*., 2011; Picco *et al*., 2012a, 2012b; Kaless *et al*., 2013). The flood events of November-December 2010 (RI = 8-10 years) have caused an expansion of the active channel average width by about 10% (from 196 m to 215 m) with the consequent removal of 10 ha of riparian vegetation (11% less) in the study reach (for more detailed information see Moretto *et al*., 2012a, 2012b). The sediment processes can be analysed in detail at sub-reach level thanks to the HDTMs developed with the proposed methodology.

A severe flood event seems to generate riffle-pool migrations in the case with no nearby -natural or -artificial constrictions (e.g. P1 of Friola and Fontaniva 2010), while a pool enlargement along the channel when they are beside a constriction (e.g. P4 of Nove and P3 – P4 of Friola 2011). The location and geometry of the new bed forms seem to be related to the natural (vegetated bar) and anthropic (embankments and bridges) constrictions. Comparing the 2010 and 2011 pools it can also be noted that after a severe flood event, they are generally longer and the migrations are more concentrated beside the more compact lateral sides (Figure 9). The embankments and fluvial islands seem to have played an important role in the bed-

form dynamics during the floods. Indeed, the pools of each 2011 sub-reach are located mainly next to more compact lateral surface with embankments and/or vegetated bars. On the other hand, riffles are mainly located over old pools and where no significant "constrictions" were present on either side of the wet areas.

The different behaviour of the three sub-reaches seems to be attributable to their diverse morphological characteristics (natural and imposed) and the availability of sediment from the upstream reach (Moretto *et al*., 2012a, 2012b, 2013b). The first sub-reach is the most studied and the most affected by erosion processes (Moretto *et al*., 2012a). The conditions of Nove sub-reach can be summarized as follows: i) past and present heavy incision of the active channel with modifications in section shape and from the river basin; ii) very little sediment supply from upstream reaches; iii) almost total absence of vegetation on the floodplain; iv) increase of local slope.

In the second sub-reach, Friola, the Brenta River has a lower slope and is less constrained laterally than in the upstream area, as confirmed by the presence of a large island and a secondary channel to the right. During severe floods, therefore, the main channel can migrate forming new deposition bars. On the other hand the dynamics of Fontaniva are related to: i) greater availability of eroded sediments coming from the upper sub-reaches; ii) more balanced erosion deposition pattern (Moretto *et al*., 2012a, 2012b, 2013b); iii) increase in the average elevation of the active channel in the last 30 years; iv) presence of extended and stable vegetation in the floodplain area which is increasingly affected by flood events; v) reduction of local slope; vi) presence of infrastructures (2 bridges). The slope reduction, together with the increase in average elevation of the active channel in the last 30 years (Moretto *et al*., 2012a, 2012b, 2013b), determine a greater spatial mobility of the flood flow than in the past (with RI > 5 years), above all in external areas where dense and stable riparian vegetation is present (Figure 1). This means increased roughness and a river slowdown with the reduction of transport capacity.

The morphological changes that occurred in the Brenta River as a consequence of the flood events in 2010 (RI of about 8 and 10 years) are of great importance to evaluate the fluvial hydro-morphological quality, because they highlight the processes that are taking place, and provide insights into their future evolution as required by the EU Water Framework Directive. Nevertheless, for implementing evolutionary models and estimating sediment transport, a better assessment of the quantity of incoming and outbound sediment in the study reach and a detailed analysis of the transport rate in relation to the event magnitude are needed. Several works apply the morphological approach for estimating the sediment budget starting from transversal sections (i.e. Lane, 1998; Surian and Cisotto, 2007, Bertoldi *et al*., 2010), nonetheless a much more accurate spatial definition can be obtained from remote sensing data (i.e. Hicks *et al*., 2006; Hicks, 2012; Rennie, 2012; Milan and Heritage, 2012). The traditional methodologies of terrain change detection (e.g. with dGPS cross-sections) report a high precision punctual definition, however the determination of volume changes at reach scale may be improved with the assessment of DEMs differences (Lane *et al*., 2003). The implementation of LiDAR data and colour bathymetry with the proposed methodology allowed us to obtain a terrain digital model with sufficient accuracy to derive patterns of sediment transfer, in particular within the water channels. The information obtained from such an analysis should be integrated with direct field measurements.

6. FINAL REMARKS

The proposed methodology allows high-resolution DTMs of wet areas to be produced with an associated uncertainty that has proved to be comparable to the LiDAR data. The bathymetric model calibration requires only a dGPS survey in the wet areas contemporary to aerial image acquisition. Statistical analyses have demonstrated both that all three colour bands (R, G, B) significantly correlate with water depth and a good performance of the empirical models. In

addition the presence of an interaction between the colour bands cannot be neglected.

Error sources (reflections, turbulences, strong colour variations at the bottom, shadows, suspended load, exposed sediment, etc.) were mostly intercepted through the two proposed filters for the curvature assessment and eliminating the implausible upper and lower limits in the bathymetric raster. The validation of the Hybrid Digital Terrain Models (HDTM) resulted as being satisfactory for distributed evaluations of morphological variations.

If the aim is to quantify erosion-deposition patterns, apply numerical models or develop sediment budgets, as demonstrated in table 1, the bathymetric methods are fundamental to obtain realistic evaluations.

The flood events of November-December 2010 (RI= 8 and 10 years) have caused significant geomorphic changes in the three sub-reaches. The different behaviour of the sub-reaches seems to be attributable to their diverse morphological characteristics (natural and imposed) and the availability of sediment from the upstream reach.

The riffle-pool dynamics seems not be casual, but influenced by the natural (vegetated bar) and anthropic (embankments and bridges) constrictions. After a severe flood event, the pools seem be located mainly on the side of the wet area with a more compact lateral surface with embankments and/or vegetated bars. On the other hand, riffles seem be located mainly where no significant “constrictions” were present on either side of the wet areas.

The results of this study can be a valuable support to generate precise elevation models also for wet areas, useful for evaluating erosion-deposition patterns, improving sediment budget calculations and the implementation of 2D and 3D numerical hydrodynamic models.

Notation

dGPS	Differential Global Positioning System
DEM	Digital Elevation Model
DPH	Channel Depth
DTM	Digital Terrain Model
HDTM	Hybrid Digital Terrain Model
LiDAR	Light Detection And Ranging
RDPH	Raw channel depth model (raster and/or points)
RGB	Red Green Blue
RI	Recurrence Interval
Zdry	Z coordinate of dry area
Zwet	Z coordinate of wet area
Zwl	Z coordinate of water level

ACKNOWLEDGEMENTS

This research was funded by the CARIPARO Research Project “Linking geomorphological processes and vegetation dynamics in gravel-bed rivers”; the University of Padua Strategic Research Project PRST08001, “GEORISKS, Geological, morphological and hydrological processes: monitoring, modelling and impact in North-Eastern Italy”, Research Unit STPD08RWBY-004; the Italian National Research Project PRIN20104ALME4-ITSedErosion: “National network for monitoring, modeling and sustainable management of erosion processes in agricultural land and hilly-mountainous area"; and the EU SedAlp Project: "Sediment management in Alpine basins: Integrating sediment continuum, risk mitigation and hydropower", 83-4-3-AT, within the framework of the European Territorial Cooperation Programme Alpine Space 2007-2013. All colleagues and students who helped in the field are sincerely thanked. Thanks to mother language Ms Alison Garside for your efficient English correction of the final English version and for your final check of the paper.

REFERENCES

Ashmore, P.E., Church, M.J., 1998. Sediment transport and river morphology: a paradigm for study. In Kingleman, P.C., Bechta, R.L., Komar, P.D., and Bradley, J.B. (eds.) *Gravel Bed Rivers in the Environment.* Highland Ranch, CO, Water Resources Publications, pp. 115-148.

Bathurst, J.C., Crosta, G.B., Garcìa Ruiz, J.M., Guzzetti, F., Lenzi, M.A., Aragues, S., 2003. Debris fall assessment in mountain catchments for local End-users. *International Conference on Debris Flow Hazards Mitigation: Mechanics, Prediction and Assessment,* Proceedings 2, pp. 1073-1083.

Bertoldi, W., Gurnell, A., Surian, N., Tockner, K., Zanoni, L., Ziliani, L., Zolezzi, G., 2009. Understanding reference processes: linkages between river flows, sediment dynamics and vegetated landforms along the Tagliamento River, Italy. *River Research and Applications* **25**: 501–516.

Bertoldi, W., Zanoni, L., Tubino, M., 2010. Assessment of morphological changes induced by flow and flood pulses in a gravel bed braided river: the Tagliamento River (Italy). *Geomorphology* **114**: 348–360.

Buffington, J.M., 2012. Change in channel morphology over human time scales. In Church M., Biron P.M., and Roy A.G. (eds.) *Gravel-bed Rivers: Processes, Tool, Environments*. Wiley-Blackwell, pp. 435-463.

Burnham, K.P., Anderson, D.R., 2002. Model Selection and Multimodel Inference: A Practical Information-Theoretic Approach, 2nd ed. *Springer* **16**, pp. 488.

Carbonneau, P.E., Lane, S.N., Bergeron, N.E., 2006. Feature based image processing methods applied to bathymetric measurements from airborne remote sensing in fluvial environments. *Earth Surface Processes and Landforms* **31**: 1413–1423; doi: 10.1002/ esp. 1341.

666 Comiti, F., 2011. How natural are Alpine mountain rivers? Evidence from the Italian Alps.
667 *Earth Surface Processes and Landforms* **37**, *693-707;* doi: 10.1002/esp.2267
668 Comiti, F., Da Canal, M., Surian, N., Mao, L., Picco, L., Lenzi, M.A., 2011. Channel
669 adjustments and vegetation cover dynamics in a large gravel bed river over the last 200
670 years. *Geomorphology* **125**: 147-159.
671 Conesa-Garcìa, C., Lenzi, M.A., 2010. Check Dams, Morphological Adjustments and Erosion
672 Control in Torrential Streams (eds.). *Nova Science Publishers*, New York, pp. 298.
673 Dixon, L.F.J., Barker, R., Bray, M., Farres, P., Hooke, J., Inkpen, R., Merel, A., Payne, D.,
674 Shelford, A., 1998. Analytical photogrammetry for geomorphological research. In Lane
675 S.N., Richards K.S., Chandler J.H. (eds.). *Landform Monitoring, Modelling and Analysis,*
676 John Wiley & Sons: Chichester; Chapter 4, pp. 63–94.
677 Dierssen, H.M., Zimmerman, R.C., Leathers, R.A., Downes, T.V., Davis, C.O., 2003. Ocean
678 color remote sensing of seagrass and bathymetry in the Bahamas Banks by high-resolution
679 airborne imagery. *Limnology and Oceanography* 48(1, part 2): 444–455.
680 Fryer, J.G., 1983. A simple system for photogrammetric mapping in shallow-water.
681 *Photogrammetric Record* **11**: 203–208.
682 Heritage, G.L., Fuller, I.C., Charlton, M.E., Brewer, P.A., Passmore, D.P., 1998. CDW
683 photogrammetry of low relief fluvial features: accuracy and implications for reach-scale
684 sediment budgeting. *Earth Surface Processes and Landforms* **23**: 1219–1233.
685 Hicks, D.M., Duncan, M.J., Walsh, J.M., Westaway, R.M., Lane S.N., 2002. New views of
686 the morphodynamics of large braided rivers from high-resolution topographic surveys and
687 time-lapse video. *IAHS Publication* **276**: 373–380.
688 Hicks, D.M., Shankar, U., Duncan, M.J, Rebuffe, M., Abele, J., 2006. Use of remote sensing
689 technologies to assess impacts of hydro-operations on a large, braided, gravel-bed river:
690 Waitaki River, New Zealand. In Sambrook Smith G.H., Best J.L., Bristow C.S., Petts G.E.,

(eds.) *Braided Rivers, Processes, Deposits, Ecology and Management.* International Association of Sedimentologists, Special Publication 36, Blackwell: Oxford. pp. 311-326.

Hicks, D.M., 2012. Remotely sensed topographic change in gravel riverbeds with flowing channels. In Church M., Biron P.M., and Roy A.G. (eds.) *Gravel-bed Rivers: Processes, Tool, Environments*. Wiley-Blackwell, pp. 303-314.

Hilldale, R.C., Raff, D., 2008. Assessing the ability of airborne LiDAR to map river bathymetry. *Earth Surface Processes and Landforms* **33**: 773-783.

Kaless, G., Mao, L., Lenzi, M.A., 2011. Regime theories in gravel bed rivers; preliminary comparison between disturbed rivers due to antrophic activities (Northeastern Italy) and natural rivers (Patagonia, Argentina). *Proceedings of the Intermediate Congress of the Italian Association of Agricultural Engineering*; Belgirate, Italy; September 22-24, 2011; pp. 8.

Kaless, G., Mao, L., Lenzi, M.A., 2013. Regime theories in gravel bed rivers: models, controlling variables, and applications in disturbed Italian rivers. *Hydrological Processes;* doi: 10.1002/hyp.9775

Kinzel P.J., Wright C.W., Nelson J.M., Burman A.R., 2007. Evaluation of an experimental LiDAR for surveying a shallow, braided, sand-bedded river. *Journal of Hydraulic Engineering* **133**: 838–842.

Kinzel, P. J., Legleiter, C. J., Nelson, J. M., 2013. Mapping River Bathymetry With a Small Footprint Green LiDAR: Applications and Challenges. *Journal of the American Water Resources Association (JAWRA)* **49**: 183–204. doi: 10.1111/jawr.12008

Lane, S.N., 1998. The use of digital terrain modelling in the understanding of dynamic river channel systems. In Lane S.N., Richards K., Chandler J. (eds.), *Landform Monitoring, Modelling and Analysis*. Wiley, Chichester; pp. 311–342.

715 Lane, S.N., Richards, K.S., Chandler, J.H., 1994. Developments in monitoring and terrain
716 modelling of small-scale riverbed topography. *Earth Surface Processes and Landforms* **19**:
717 349–368.
718 Lane, S.N., Westaway, R.M., Hicks, D.M., 2003. Estimation of erosion and deposition
719 volumes in a large, gravel-bed, braided river using synoptic remote sensing. *Earth Surface*
720 *Processes and Landforms* **28**(3):249–271; DOI: 10.1002/esp.483.
721 Lane, S.N., Tayefi, V., Reid S.C., Yu D., Hardy, R.J., 2007. Interactions between sediment
722 delivery, channel change, climate change and flood risk in a temperate upland
723 environment. *Earth Surface Processes and Landforms* **32**: 429–446.
724 Lane, S.N., Widdison, P. E., Thomas, R.E., Ashworth, P.J., Best, J.L., Lunt, I.A., Sambrook
725 Smith, G.H., Simpson, C.J., 2010. Quantification of braided river channel change using
726 archival digital image analysis. *Earth Surface Processes and Landforms* **35**: 971–985.
727 DOI: 10.1002/esp.2015.
728 Legleiter, C.J., 2011. Remote measurement of river morphology via fusion of LiDAR
729 topography and spectrally based bathymetry. *Earth Surface Processes and Landforms* **37**:
730 499-518.
731 Legleiter, C.J., Roberts, D.A., 2009. A forward image model for passive optical remote
732 sensing of river bathymetry. *Remote Sensing of Environment* **113**: 1025–1045.
733 Legleiter, C.J., Roberts, D.A., Marcus, W.A., Fonstad, M.A., 2004. Passive optical remote
734 sensing of river channel morphology and in-stream habitat: Physical basis and feasibility.
735 *Remote Sensing of Environment* **93**: 493-510.
736 Legleiter, C.J., Roberts, D.A., Lawrence, R.L., 2009. Spectrally based remote sensing of river
737 bathymetry. *Earth Surface Processes and Landforms* **34**: 1039–1059.
738 Legleiter, C.J., Kinzel, P.J., Overstreet, B.T., 2011. Evaluating the potential for remote
739 bathymetric mapping of a turbid, sand-bed river: 1. Field spectroscopy and radiative
740 transfer modeling. *Water Resour. Res*., **47**, W09531, doi:10.1029/2011WR010591.

741 Legleiter, C.J., 2013. Mapping river depth from publicly available aerial images. *River*
742 *Research and Applications* **29**: 760–780. doi: 10.1002/rra.2560
743 Lindsay, J.B., Ashmore, P.E., 2002. The effects of survey frequency on estimates of scour and
744 fill in a braided river model. *Earth Surface Processes and Landforms* **27(1)**: 27–43.
745 Lenzi, M.A., Mao, L., Comiti, F., Rigon, E., Picco, L., Vitti, P., Moretto, J., Sigolo, C., 2010.
746 Scientific contribution by the Research Unit Land and Agro-forest Department, to the
747 research activities carried out in the framework of the CARIPARO Project "Linking
748 geomorphological processes and vegetation dynamics in gravel-bed rivers", from
749 September 2009 to October 2010. *Research and Technical Report; Department of Land*
750 *and Agro-forest Environment, University of Padova, Padova , Italy*, pp. 102.
751 Lenzi, M.A., D'Agostino, V., Gregoretti, C., Sonda, D., 2003. A simplified numerical model
752 for debris-flow hazard assessment: DEFLIMO. *International Conference on Debris Flow*
753 *Hazards Mitigation: Mechanics, Prediction and Assessment, Proceedings* 1, pp. 611-622.
754 Lenzi, M.A., 2006. Research developments in debris flow monitoring, modeling and hazard
755 assessment in Italian mountain catchments. *WIT Transactions on Ecology and the*
756 *Environment* **90**: 135-145.
757 McKean, J.A., Nagel, D., Tonina, D., Bailey, P., Wright, C.W., Bohn, C., Nayegandhi, A.,
758 2009. Remote sensing of channels and riparian zones with a narrow-beam aquatic-
759 terrestrial LIDAR. *Remote Sensing* **1(4)**:1065-1096.
760 Macklin, M.G., Rumsby, B.T., 2007. Changing climate and extreme floods in the British
761 uplands. *Transactions of the Institute of British Geographers*, 32, pp. 168–186. doi:
762 10.1111/j.1475-5661.2007.00248.x
763 Mao, L., Lenzi, M.A., 2007. Sediment mobility and bedload transport conditions in an alpine
764 stream. *Hydrological Processes*, **21**(14): 1882-1891.

765 Mao, L., Cavalli, M., Comiti, F., Marchi, L., Lenzi, M.A., Arattano, M., 2009. Sediment
766 transfer processes in two Alpine catchments of contrasting morphology settings. *Journal of*
767 *Hydrology* **364**: 88-98.
768 Marcus, W.A., 2012. Remote sensing of the hydraulic environments in gravel-bed rivers. In
769 Church M., Biron P.M., and Roy A.G. (eds.) *Gravel-bed Rivers: Processes, Tool,*
770 *Environments*. Wiley-Blackwell, pp. 261-285.
771 Marcus, W.A., Fonstad, M.A., 2008. Optical remote mapping of rivers at sub-meter
772 resolutions and watershed extents. *Earth Surface Processes and Landforms* **33**: 4–24.
773 Marcus, W.A., Legleiter, C.J., Aspinall, R.J., Boardman J.W., Crabtree R.L., 2003. High
774 spatial resolution hyperspectral mapping of in-stream habitats, depths, and woody debris in
775 mountain streams. *Geomorphology* **55**: 363–380.
776 Milan, D.J., Heritage, G.L., Hetherington, D., 2007. Application of a 3D laser scanner in the
777 assessment of erosion and deposition volumes and channel change in a proglacial river.
778 *Earth Surface Processes and Landforms* **32**: 1657–1674.
779 Milan, D.J., Heritage, G.L., 2012. LiDAR and ADCP use in gravel-bed rivers: Advances
780 since GBR6. In Church M., Biron P.M., and Roy A.G. (eds.) *Gravel-bed Rivers:*
781 *Processes, Tool, Environments*. Wiley-Blackwell, pp. 286-302
782 Milan, D.J., Heritage, G.L., Large, A.R.G., Fuller, I.C., 2011. Filtering spatial error from
783 DEMs: Implications for morphological change estimation. *Geomorphology* **125**: 160-171.
784 Moretto, J., Delai, F., Picco, L., Lenzi, M.A., 2013a. Integration of colour bathymetry,
785 LiDAR and dGPS surveys for assessing fluvial changes after flood events in the
786 Tagliamento River (Italy). *Agricultural Sciences* 4(8A): 21-29;
787 doi: 10.4236/as.2013.48A004
788 Moretto, J., Rigon, E., Mao, L., Picco, L., Delai, F., Lenzi, M.A., 2013b. Channel adjustment
789 and island dynamics in the Brenta River (Italy) over the last 30 years. *River Research and*
790 *Applications;* doi: 10.1002/rra.2676

Moretto, J., Rigon, E., Mao, L., Picco, L., Delai, F., Lenzi, M.A., 2012a. Assessing short term erosion-deposition processes of the Brenta River using LiDAR survey. *WIT Transactions on Engineering Sciences* **73**: 149-160; doi: 102495/DEB120131.

Moretto, J., Rigon, E., Mao, L., Picco, L., Delai, F., Lenzi, M.A., 2012b. Medium-and short-term channel and island evolution in a disturbed gravel bed river (Brenta River, Italy). *Journal of Agricultural Engineering* **43**(4); 176-188; doi: 10.4081/jae.2012.e27.

Muste, M., Kim, D., Merwade, V., 2012. Modern digital instruments and techniques for hydrodynamic and morphologic characterization of river channels. In Church M., Biron P.M., and Roy A.G. (eds.) *Gravel-bed Rivers: Processes, Tool, Environments*. Wiley-Blackwell, pp. 315-341.

Panissod, F., Bailly, J.S., Durrieu, S., Jacome, A., Mathys, N., Cavalli, M., Puech, C., 2009. Qualifiction de modeles numeriques de terrain Lidar pour l'etude de l'erosion: Application aux badlands de draix. *Revue Francaise de Photogrammetrie et de Teledetection* **192**: 50-57.

Picco, L., Mao, L., Rigon, E., Moretto, J., Ravazzolo, D., Delai, F., Lenzi, M.A., 2012a. Medium term fluvial island evolution in relation with floods events in the Piave River. *WIT Transactions on Engineering Sciences*, Vol 73, 161-172; doi: 10.2495/DEB120141; ISSN 1743-3522.

Picco, L., Mao, L., Rigon, E., Moretto, J., Ravazzolo, D., Delai, F., Lenzi, M.A., 2012b. Riparian forest structure, vegetation cover and flood events in the Piave River. *WIT Transactions on Engineering Sciences* **73**: 137-147; doi: 10.2495/DEB120121; ISSN 1743-3522.

Picco, L., Mao, L., Cavalli, M., Buzzi, R., Rainato, R., Lenzi, M.A., 2013. Evaluating short-term morphological changes in a gravel-bed braided river using Terrestrial Laser Scanner. *Geomorphology*. doi.10.1016/j.geomorph.2013.07.007

816 Rennie, C.D., 2012. Mapping water and sediment flux distributions in gravel-bed rivers using
817 ADCPs. In Church M., Biron P.M., and Roy A.G. (eds.) *Gravel-bed Rivers: Processes,*
818 *Tool, Environments*. Wiley-Blackwell, pp. 342-350.
819 Rigon, E., Comiti, F., Mao, L., Lenzi, M.A., 2008. Relationships among basin area, sediment
820 transport mechanisms and wood storage in mountain basins of the Dolomites (Italian
821 Alps). WIT *Transactions on Engineering Sciences* **60**:163-172.
822 Rinner, K., 1969. Problems of two medium photogrammetry. *Photogrammetric Engineering*
823 **35**: 275.
824 Rumsby, B.T., Macklin ,M.G., 1994. Channel and floodplain response to recent abrupt
825 climate change: The Tyne basin, Northern England. *Earth Surface Processes and*
826 *Landforms* **19(6)**: 499–515.
827 Rumsby, B.T., Brasington, J., Langham, J.A., McLelland, S.J., Middleton, R., Rollingson, G.,
828 2008. Monitoring and modelling particle and reach-scale morphological change in gravel-
829 bed rivers: Applications and challenges. *Geomorphology* **93(1)**: 40-54.
830 Stover, S.C., Montgomery D.R., 2001. Channel change and flooding, Skokomish River,
831 Washington. *Journal of Hydrology* **243**: 272-286.
832 Surian, N., Cisotto, A., 2007. Channel adjustments, bedload transport and sediment sources in
833 a gravel-bed river, Brenta river, Italy. *Earth Surface Processes and Landforms* **32**: 1641-
834 1656.
835 Surian, N., Ziliani, L., Comiti, F., Lenzi, M.A., Mao, L., 2009. Channel adjustments and
836 alteration of sediment fluxes in gravel-bed rivers of north-eastern Italy: Potentials and
837 limitations for channel recovery. *River Research and Applications* **25**: 551-567.
838 Surian, N., 2012. Field observations of gravel-bed river morphodynamics: perspectives and
839 critical issues for testing of models. In Church M., Biron P.M., and Roy A.G. (eds.)
840 *Gravel-bed Rivers: Processes, Tool, Environments*. Wiley-Blackwell, pp. 90-95.

Taylor, J., 1997. An Introduction to Error Analysis: the Study of Uncertainties in Physical Measurements. (2nd ed.) *University Science Books*: Sausalito, CA.

Winterbottom, S.J., Gilvear, D.J., 1997. Quantification of channel bed morphology in gravel-bed rivers using airborne multispectral imagery and aerial photography. *Regulated Rivers: Research and Management* **13**: 489–499.

867 **Table 1** Estimated uncertainty for HDTM and DoD models.

		NOVE		FRIOLA		FONTANIVA	
		2010	2011	2010	2011	2010	2011
HDTM area	(m^2)	566916	566916	836967	836967	627049	627049
Wet area	(m^2)	76463	76526	108265	119497	75545	97407
Wet area/HDTM area		0.13	0.13	0.13	0.14	0.12	0.16
N° dGPS point for test DTM_{BTH}		192	408	279	821	204	283
Average uncertainty DTM_{BTH} + dGPS	(m)	0.26	0.26	0.25	0.19	0.26	0.26
N° dGPS point for test DTM_{LD}		72	132	98	155	53	64
Average uncertainty DTM_{LD} + dGPS	(m)	0.14	0.15	0.24	0.15	0.26	0.16
TOTAL average uncertainty	(m)	0.16	0.16	0.24	0.16	0.26	0.17
Volume loss without colour bathymetry	(m^3)	917559	529812	1206848	397470	4386814	4743783

868

869 DTM_{BTH}: Part of Digital Elevation Model derived by Bathymetry; DTM_{LD}: Part of
870 Digital Elevation Model derived by Light Detection and Ranging; dGPS: Differential
871 Global Positioning System.

872

873

874

875

876

877

878

879

880

881

882

883 **Table 2** Error analysis of depth-colour models at different water stages for 2010 and 2011.
884 The average error and standard deviation have been weighted with the corrispondence
885 inference area.

2010)

Depth	**Surface covered**		**DPH (R, G, B)**		**Calibration**
(m)	(ha)	%	error (m)	St. dev. (m)	**points**
0.00 - 0.19	20.07	34.0	0.26	0.22	107
0.20 - 0.39	14.38	24.3	0.26	0.24	87
0.40 - 0.59	13.12	22.2	0.21	0.20	75
0.60 - 0.79	8.82	14.9	0.22	0.18	59
0.80 - 0.99	2.11	3.6	0.26	0.15	32
1.00 - 1.19	0.54	0.9	0.51	0.21	20
> 1.20	0.06	0.1	0.69	0.14	13
TOTAL	**59.09**	**100**	**0.25**	**0.21**	**393**

2011)

Depth	**Surface covered**		**DPH (R, G, B)**		**Calibration**
(m)	(ha)	%	error (m)	St. dev. (m)	**points**
0.00 - 0.19	0.37	0.5	0.27	0.11	61
0.20 - 0.39	5.16	7.1	0.18	0.11	248
0.40 - 0.59	18.17	25.0	0.13	0.11	427
0.60 - 0.79	19.79	27.3	0.14	0.13	343
0.80 - 0.99	14.35	19.8	0.24	0.19	187
1.00 - 1.19	6.85	9.4	0.32	0.19	100
1.20 - 1.39	4.13	5.7	0.40	0.13	35
> 1.40	3.73	5.1	0.56	0.10	20
TOTAL	**72.53**	**100**	**0.21**	**0.14**	**1421**

886
887
888
889
890
891
892
893
894

895 **FIGURE CAPTIONS**

896

897 **Figure 1.** General view of the Brenta river and the study reaches: Nove, Friola and
898 Fontaniva.

899

900 **Figure 2.** Hydrographs of the study period (average daily discharges as measured at
901 the Barzizza gauging station).

902

903 **Figure 3.** The Brenta river at the Friola reach during the November 2010 flood event.

904

905 **Figure 4.** HDTM creation process: (A) LiDAR data and field survey, (B) data
906 preparation for process application, (C) bathymetric model determination, (D) hybrid
907 DTM creation, (E) DTM validation.

908

909 **Figure 5.** Correlation between Red, Green and Blue colour bands.

910

911 **Figure 6.** Model application (2) at Friola sub-reach (2011). The brown zones on the
912 left side are due to the presence of periphyton on the channel bottom.

913

914 **Figure 7.** Hybrid Digital Terrain Models (HDTM) of Nove, Friola and Fontaniva sub-
915 reaches, 2010 and 2011, cell size 0.5 x 0.5 m.

916

917 **Figure 8.** Cross-section comparison between dGPS, HDTM and LiDAR survey of Nove (a),
918 Friola (b) and Fontaniva (c) 2011.

919

Figure 9. Canopy surface models (CSM) with pools locations (P1, P2, etc.) through bathymetric raster on wet area of Nove, Friola and Fontaniva sub-reaches 2010 and 2011.

Figure 10. Example of filtering process in a cross-section of Friola 2011 sub-reach.

Short-term geomorphic analysis in a fluvial disturbed environment by fusion of LiDAR, colour bathymetry and dGPS survey

Highlights

i) Physical and Empirical relationship between channel depth and colour intensity;

ii) Factors that increase uncertainty of the final DTM;

iii) Hybrid DTMs (HDTMs) at high resolution and low uncertainty;

iv) Morphological processes in a regulated gravel-bed river after two several floods.

Figure 1

Click here to download high resolution image

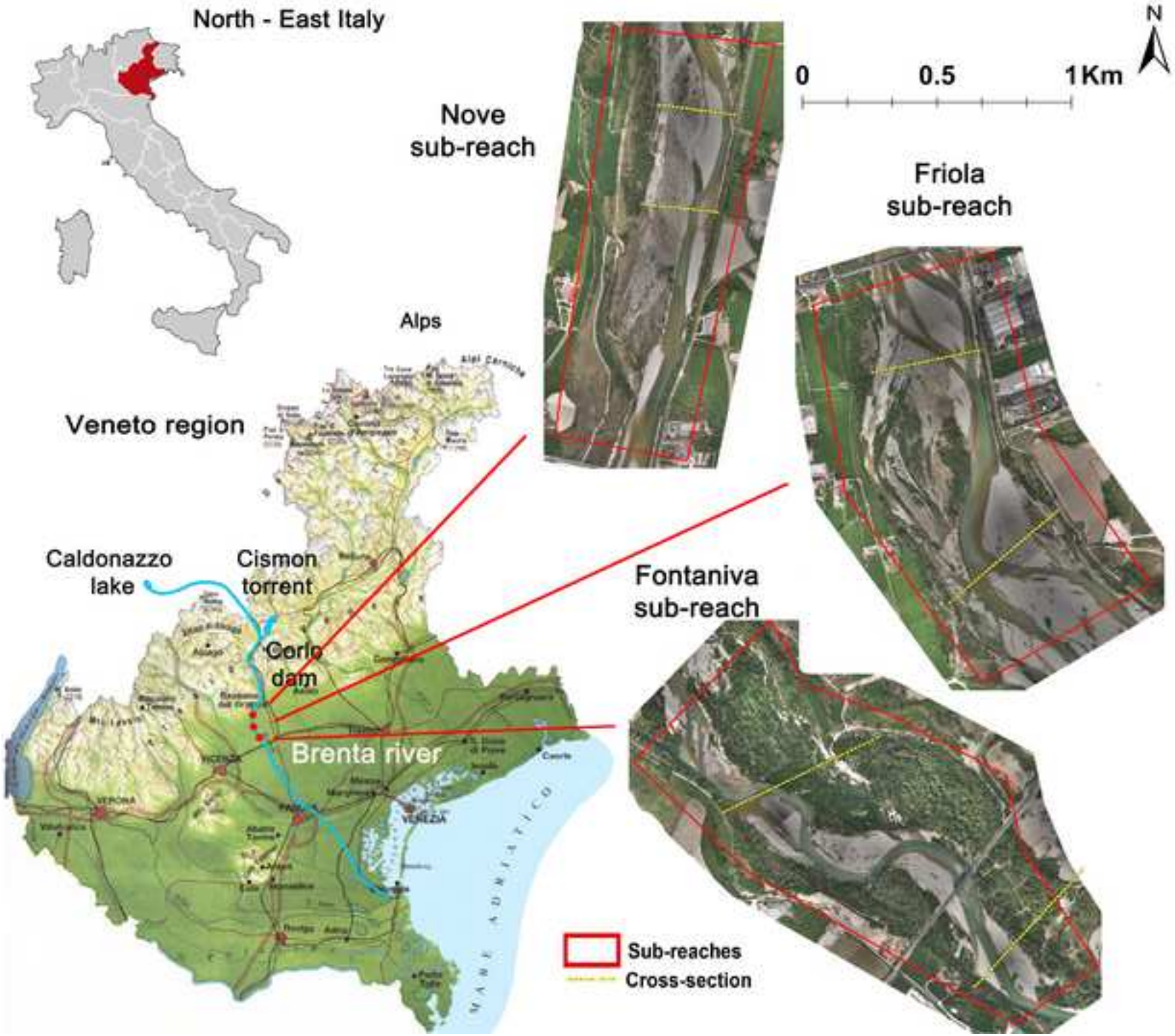

Figure 2

Click here to download high resolution image

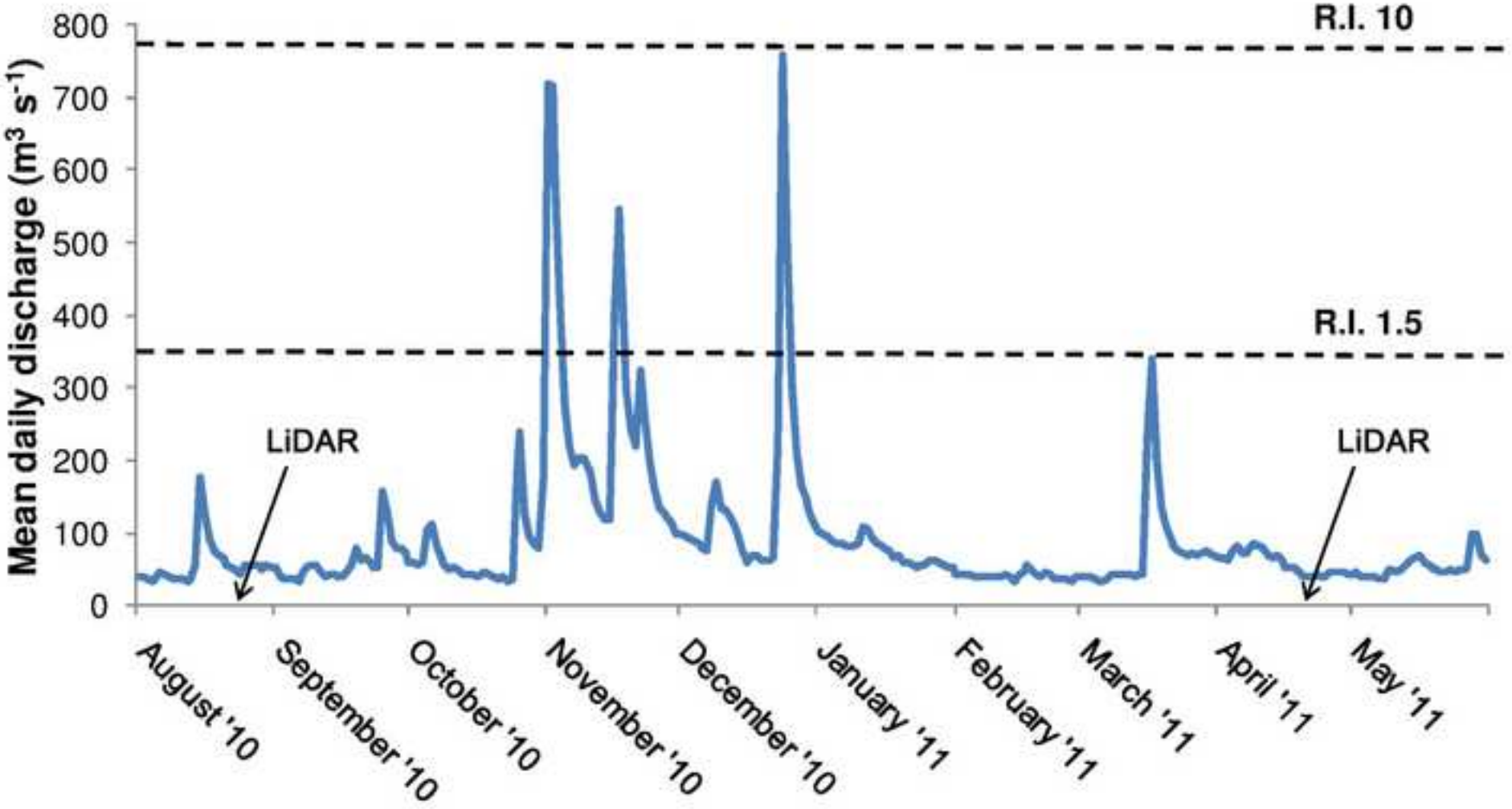

Figure 3

Click here to download high resolution image

Figure 4

Click here to download high resolution image

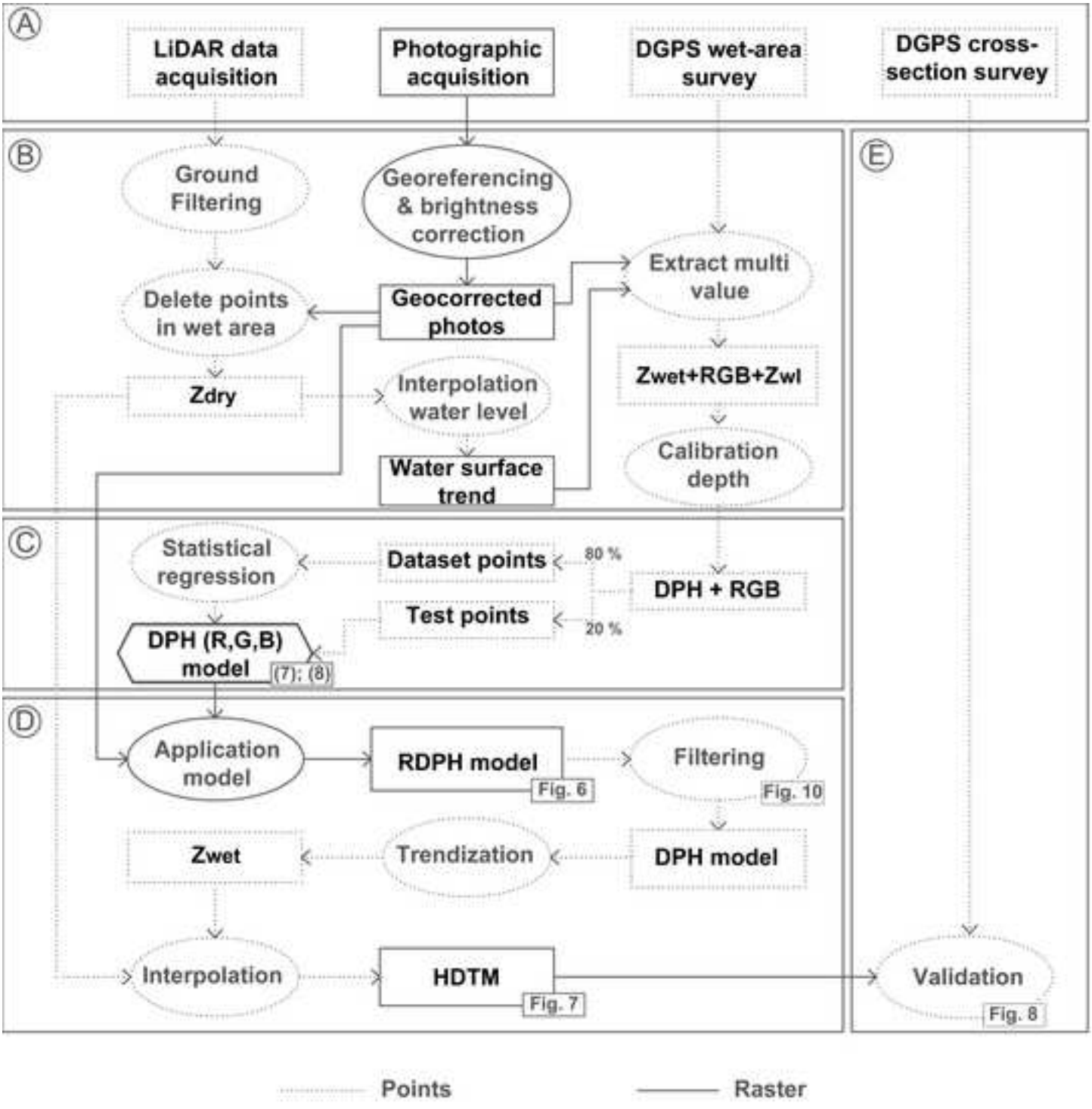

Figure 5

Click here to download high resolution image

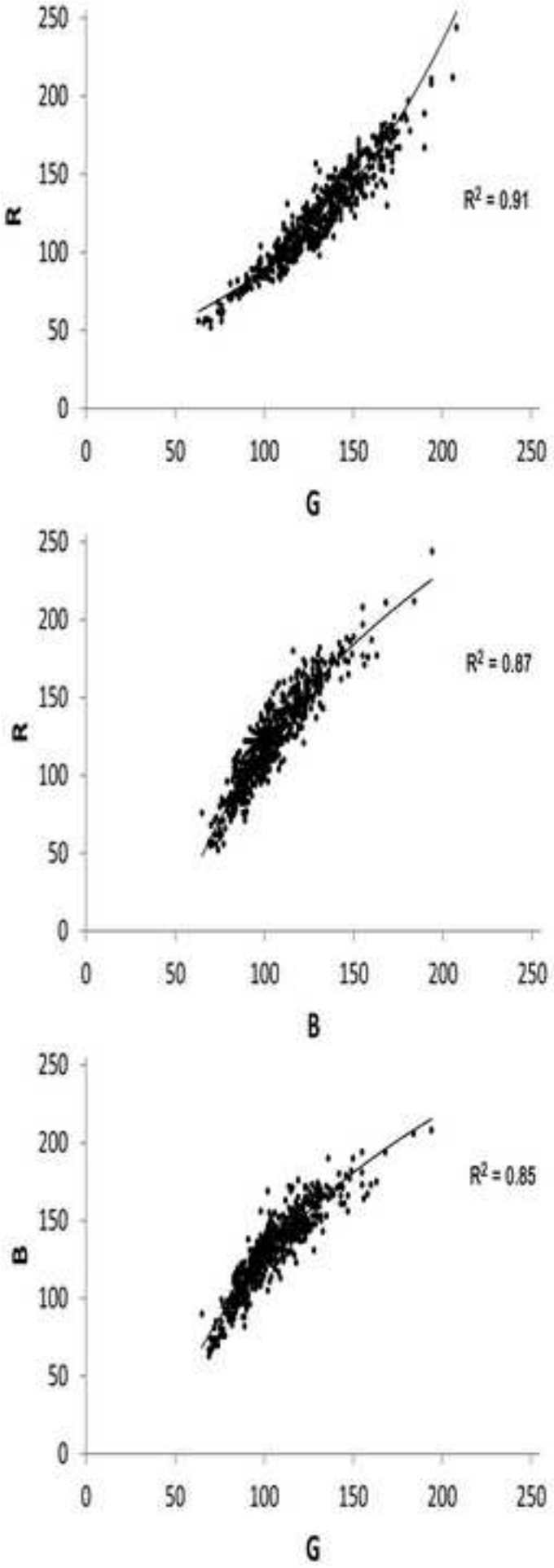

Figure 6

Click here to download high resolution image

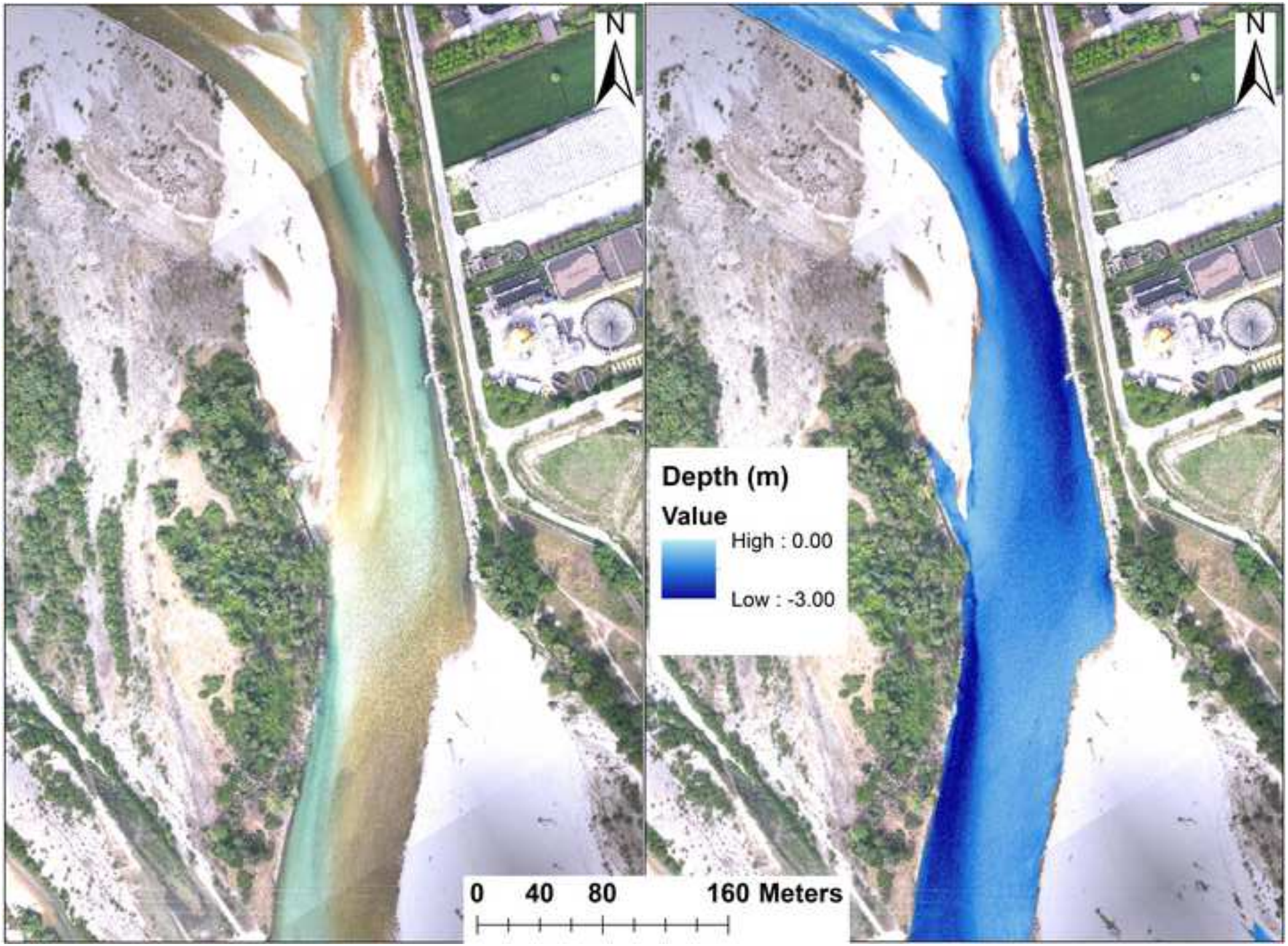

Figure 7

Click here to download high resolution image

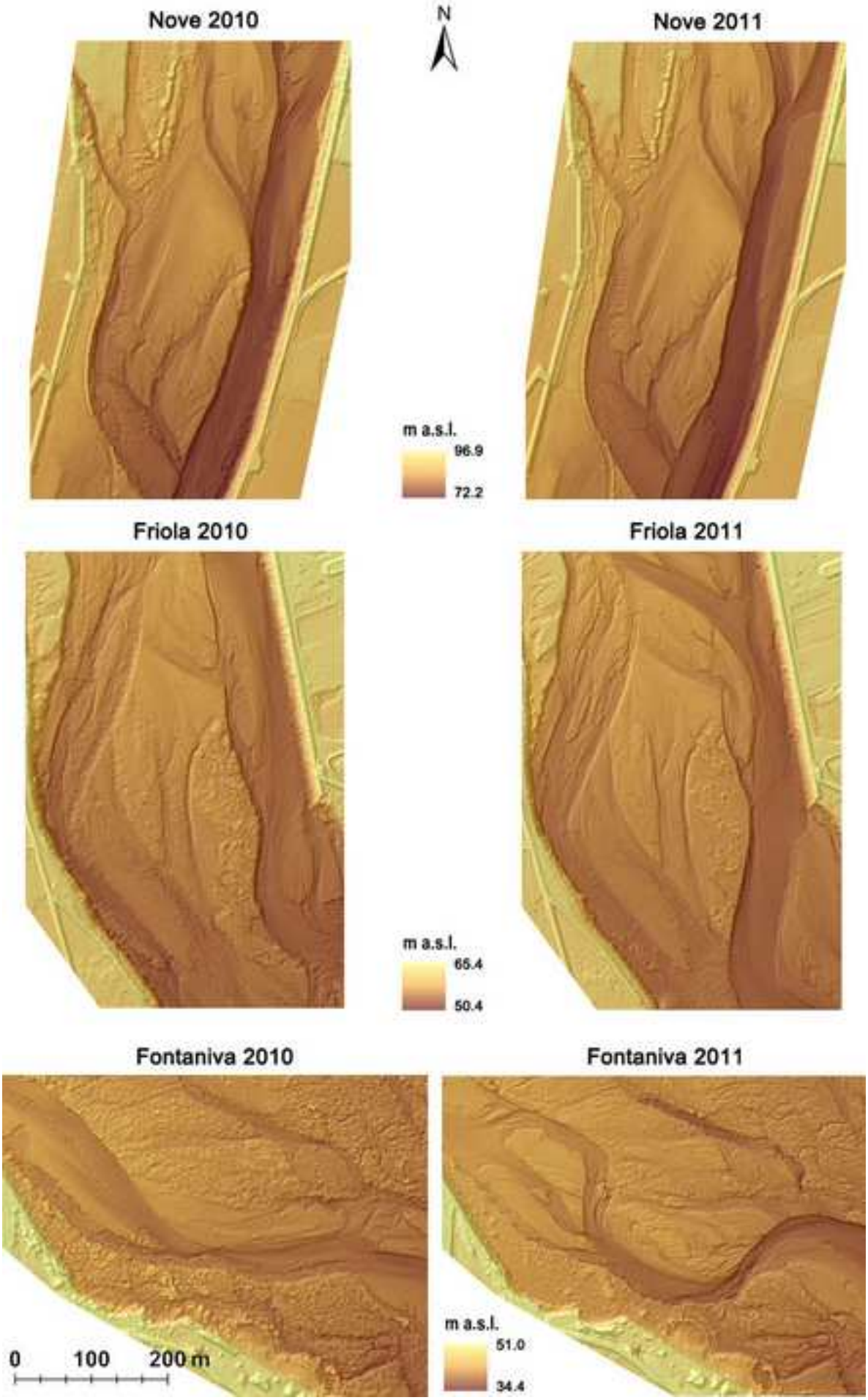

Figure 8

Click here to download high resolution image

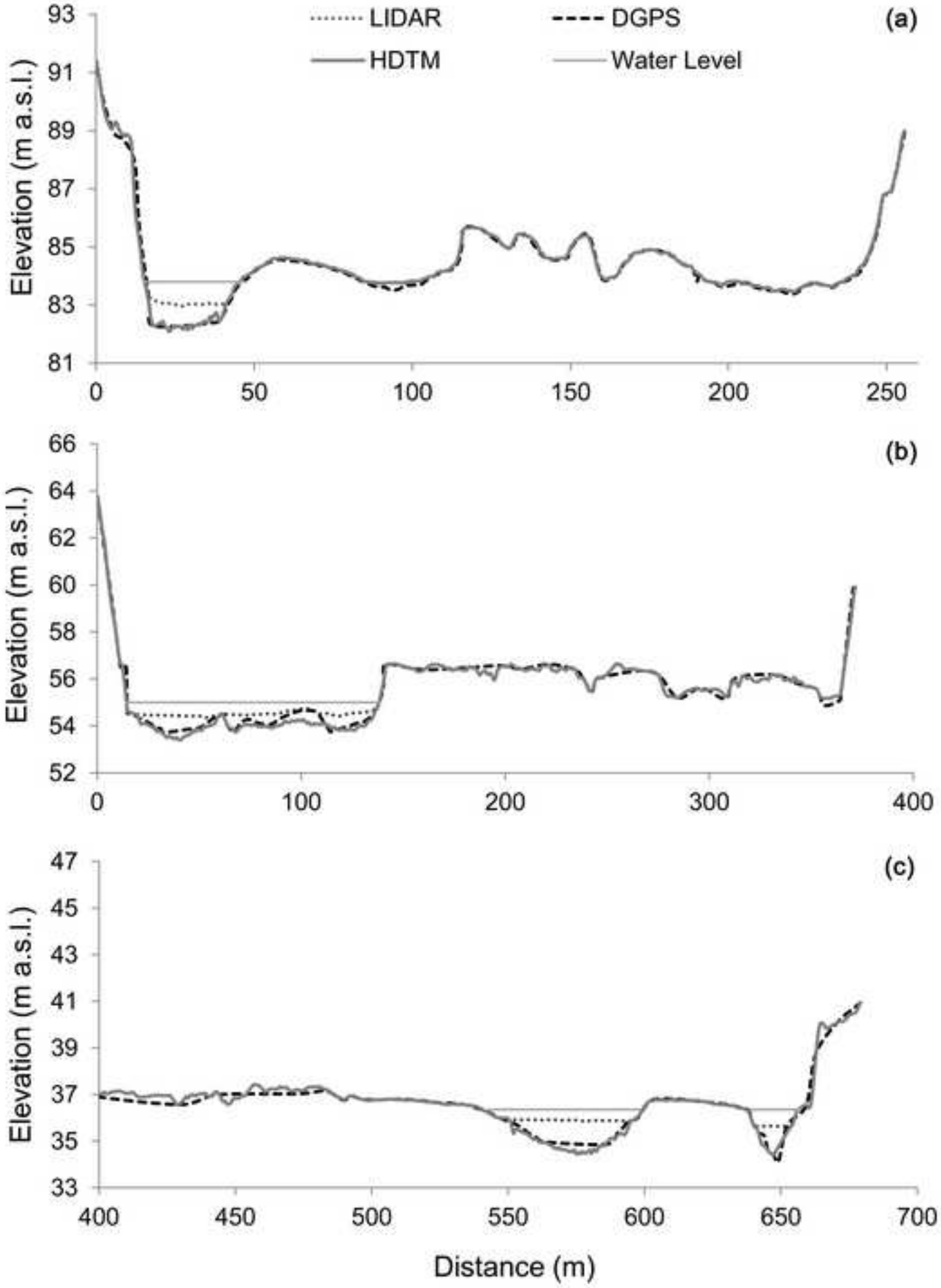

Figure 9

Click here to download high resolution image

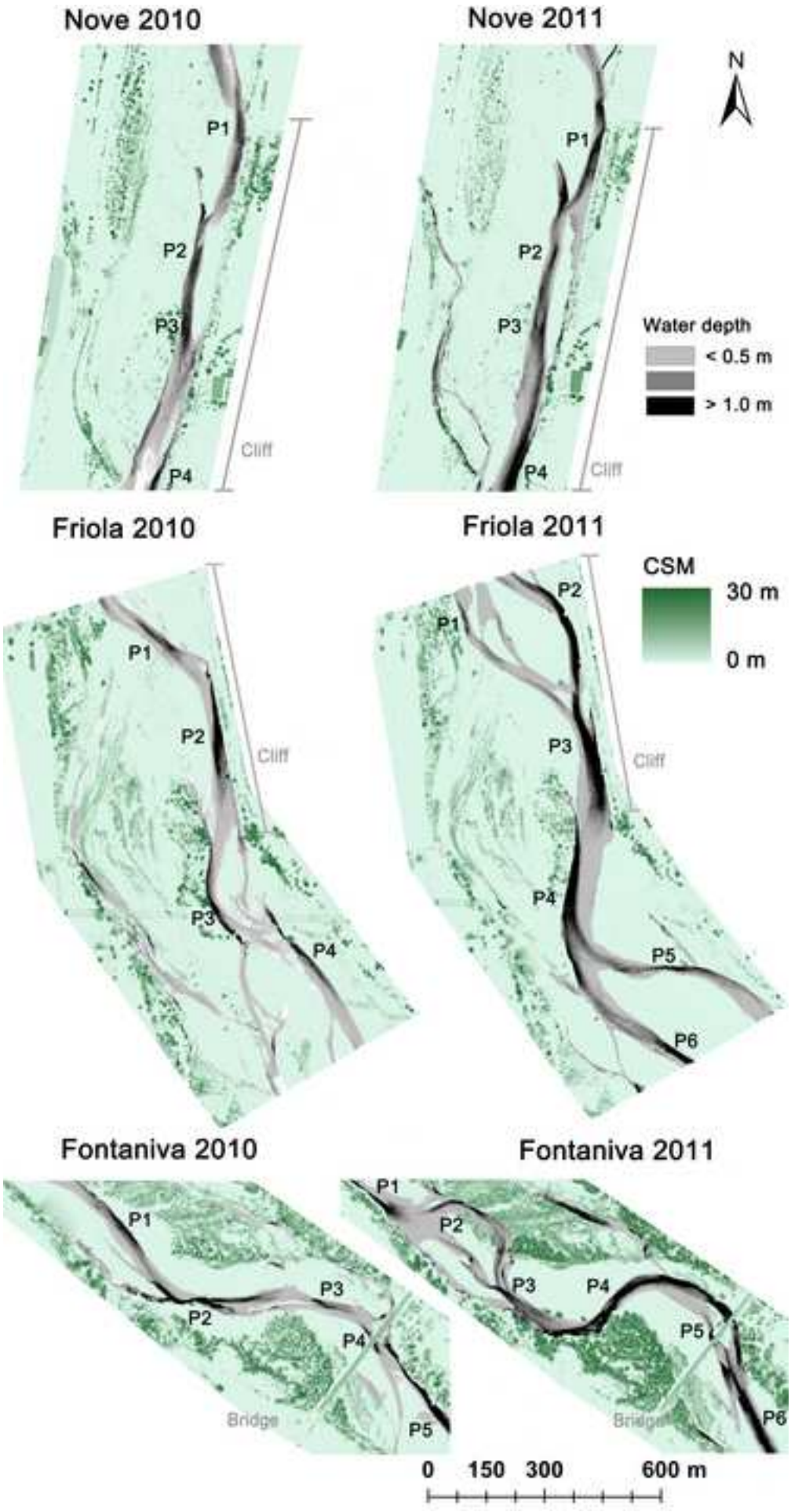

Figure 10

Click here to download high resolution image